

## Inorganic-organic hybrid nanomaterial ( $\text{Fe}_3\text{O}_4@\text{SiO}_2\text{-AQ}$ ): A retrievable heterogeneous catalyst for the green synthesis of 4*H*-chromenes

Mohammad Ali Bodaghifard<sup>a,b,\*</sup>, Zahra Mozaffari<sup>a</sup>, Zahra Faraki<sup>a</sup>

<sup>a</sup>Department of Chemistry, Faculty of Science, Arak University, Arak 38156-88138, Iran.

<sup>b</sup>Institute of Nanosciences & Nanotechnology, Arak University, Arak, Iran.

Received 7 July 2019; received in revised form 27 December 2019; accepted 16 January 2020

### ABSTRACT

Preparation of 4-aminiquinaldine grafted on silica-coated nano- $\text{Fe}_3\text{O}_4$  particles ( $\text{Fe}_3\text{O}_4@\text{SiO}_2\text{-AQ}$ ) as a novel retrievable heterogeneous nanocatalyst is described. This novel hybrid nanomaterial was applied for the green synthesis of substituted 2-amino-4*H*-chromenes via the one-pot condensation reaction of an aldehyde, malononitrile and  $\alpha$ -naphthol/ $\beta$ -naphthol/phenol under solvent-free condition. Eco-friendly method, high yield and purity of the desired products, short reaction time along with the ease of the work-up procedure outlines the advantages of these new methodologies over the earlier ones. Surface and magnetic properties of the core/shell hybrid nanoparticles were characterized via transmission electron microscopy (TEM), scanning electron microscope (SEM), X-ray powder diffraction (XRD), energy-dispersive X-ray spectroscopy (EDS), thermogravimetric analysis (TGA/DTA), and Fourier-transform infrared spectroscopy (FT-IR) techniques. This nanocatalyst can be reused at least six times without considerable loss of its performance.

**Keywords:** 4*H*-chromenes, Heterogeneous, Hybrid nanomaterial, Green synthesis.

### 1. Introduction

The reactions in which three or more starting materials react to form a product, where basically all or most of the atoms contribute to the newly formed product called multicomponent reactions (MCRs) [1]. The multicomponent reactions are a good way to produce complex and diverse combinations with high interest rates [1-3]. The MCRs have many advantages as low reaction times, diminished work-up procedures, high efficiency, cheapness, high selectivity, low environmental impact compared to different methods of classical chemistry [3,4]. MCRs are mostly experimentally simple to perform, often without the need of dry conditions and inert atmosphere. Recently MCRs provide a huge chemical diversity and currently more than hundreds different structurally varied chemical scaffolds have been described in the chemical literature [5,6].

4*H*-chromenes have attracted considerable interest due to their wide range of biological and pharmaceutical properties, including antimicrobial, antiviral, spasmolytic, diuretic, anticoagulant, anti-tumor, anti-anaphylactic and anti-proliferation activity [7-13]. In recent years, many catalysts and various methods have been reported for the synthesis of chromene derivatives [14-22, 25]. However, these methods have some disadvantages including long reaction times, harsh reaction conditions, use of toxic catalysts or solvents and boring work-up procedures. In order to avoid these limitations, scientists have intensely focused on developing clean, efficient and facile processes and reusable catalysts for synthesis of these pharmaceutically important 4*H*-chromenes.

The nanoparticles have high surface areas and do not have more of the above-mentioned disadvantages. In the other hands, the magnetic nanoparticles (MNPs) not only have high surface areas but also, they can be easily separated by using an external magnetic field and do not have tedious separation procedures which resulted from the small sizes of nanoparticles [23]. However,

\*Corresponding author.

Email: m-bodaghifard@araku.ac.ir;  
mbodaghi2007@yahoo.com (M.A. Bodaghifard)

magnetic nanoparticles can easily aggregate into larger clusters because of their anisotropic dipolar attraction. In addition, they have other deficiencies such as leaching under acidic conditions and being susceptible to autoxidation and toxicity. Therefore, it is necessary to protect the surface of MNPs in order to reduce these undesirable features. For this purpose, MNPs are usually coated with a polymeric or inorganic matrix [24]. Among inorganic compounds, SiO<sub>2</sub> can be a suitable candidate for protecting the surface of MNPs due to its high chemical and thermal stability and most importantly its easy modification by a wide range of functional groups, which increase chemical and colloidal stability of these compounds [25–31]. Besides, using magnetic nanoparticles as catalysts is associated with other advantages including easy synthesis and functionalization, low toxicity and low cost [25–28].

As part of our continuous effort to develop efficient heterogeneous magnetic nanocatalysts and green organic reactions [25, 32–34], herein we have reported the preparation of a novel heterogeneous magnetic nanoparticles as an impressive hybrid catalyst for the synthesis of 4*H*-chromene derivatives (Scheme 1). The presented method has considerable efficiency of the catalyst and environmental compatibility. Also, the catalyst was inexpensive and highly efficient and it could easily be recovered and reused.

## 2. Experimental

All chemicals were purchased from Merck or Acros chemical companies and used without further purification. Melting points were measured by using capillary tubes on an electro thermal digital apparatus and are uncorrected. Known products were identified by comparison of their spectral data and melting points with those reported in the literature. Thin layer chromatography (TLC) was performed on UV active aluminum backed plates of silica gel (TLC Silica gel 60 F254). <sup>1</sup>H and <sup>13</sup>C NMR spectra were recorded on a Bruker Avance 300 MHz spectrometer at 300 MHz and 75 MHz, respectively. Coupling constants, *J*, were reported in hertz unit (Hz). IR spectra were recorded on

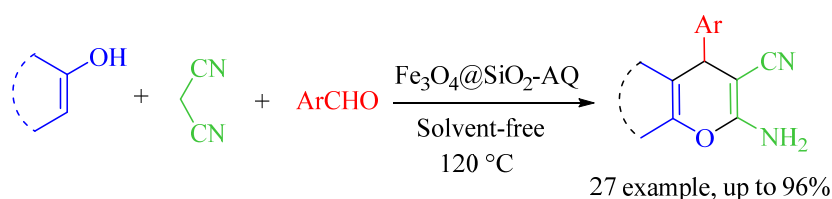
a Unicom Galaxy Series FT-IR 5030 spectrophotometer using KBr pellets and are expressed in cm<sup>-1</sup>. Elemental analyses were performed by Vario EL equipment at Arak University. X-ray diffraction (XRD) was performed on Philips XPert (Cu-K<sub>α</sub> radiation, λ = 0.15405 nm) over the range 2θ = 20–80° using 0.04° as the step length. Thermal gravimetric analysis (TGA) and differential thermal gravimetric (DTG) data for Fe<sub>3</sub>O<sub>4</sub>@SiO<sub>2</sub>-AQ were recorded on a Mettler TA4000 System under an N<sub>2</sub> atmosphere at a heating rate of 10 °C min<sup>-1</sup>. The scanning electron microscope measurement was carried out on a Hitachi S-4700 field emission-scanning electron microscope (FE-SEM).

### 2.1. Preparation of the magnetic Fe<sub>3</sub>O<sub>4</sub> nanoparticles

(MNPs) Fe<sub>3</sub>O<sub>4</sub>-MNPs were prepared using simple chemical co-precipitation method [35]. Briefly, FeCl<sub>2</sub>.4H<sub>2</sub>O (0.9941 g, 5 mmol) and FeCl<sub>3</sub>.6H<sub>2</sub>O (2.729 g, 10 mmol) were dissolved in 100 mL of deionized water in a three-necked round bottomed flask (250 mL). The mixture was heated under N<sub>2</sub> at 80 °C for 1 h, and then 10 mL of concentrated ammonia (25%) were added quickly. The solution was stirred under N<sub>2</sub> for another 1 h and then cooled to room temperature. The black precipitate formed was isolated by magnetic decantation, exhaustively washed with double-distilled water until neutrality, and further washed twice with ethanol and dried at 60 °C under vacuum.

### 2.2. Synthesis of silica-coated MNPs (Fe<sub>3</sub>O<sub>4</sub>@SiO<sub>2</sub> MNPs)

The Fe<sub>3</sub>O<sub>4</sub>@SiO<sub>2</sub> core-shell nanoparticles were prepared according to the Stober method [36]. The details are as follows: Magnetic nanoparticles MNPs (1.0 g) were homogeneously dispersed by ultrasonic vibration in a mixture of 40 mL of ethanol, 6 mL of deionized water, and 1.5 mL of 25 wt% concentrated aqueous ammonia solution, followed by the addition of 1.4 mL of tetraethylorthosilicate (TEOS). After stirring for 12 h at room temperature under an N<sub>2</sub> atmosphere, the black precipitate (Fe<sub>3</sub>O<sub>4</sub>@SiO<sub>2</sub>) was collected from the solution using a magnet, and then washed several times with water and ethanol and dried at 25 °C under vacuum.



**Scheme 1.** Fe<sub>3</sub>O<sub>4</sub>@SiO<sub>2</sub>-AQ as an efficient promoter for synthesis of 4*H*-chromene derivatives.

### 2.3. Synthesis of 3-chloropropyl-functionalized silica-coated magnetite nanoparticles ( $Fe_3O_4@SiO_2$ -PrCl MNPs)

In a typical procedure, 1.0 g of  $Fe_3O_4@SiO_2$  MNPs were dispersed in 50 mL of dry toluene using an ultrasonic bath to produce a uniform suspension, to which 2.0 g of 3-chloropropyl-trimethoxysilane (CPTMS) was added using a syringe. The resulting mixture was stirred for 24 h at 60 °C under an  $N_2$  atmosphere. Finally, the chloropropyl-functionalized solid  $Fe_3O_4@SiO_2$ -PrCl MNPs were separated using a magnet, washed with toluene, and dried under vacuum.

### 2.4. 4-Aminoquinaldine grafted on silica-coated magnetic nanoparticles ( $Fe_3O_4@SiO_2$ -AQ)

In a 100 ml round-bottomed flask,  $Fe_3O_4@SiO_2$ -PrCl nanoparticles (1.0 g) were dispersed in 50 mL toluene using an ultrasonic bath. 0.47 g 4-aminoquinaldine (3 mmol) and 0.42 g triethylamine (3 mmol) were added to the suspension. The reaction mixture was refluxed at 100 °C for 24 h. The  $Fe_3O_4@SiO_2$ -AQ MNPs were washed with hot toluene and ethanol, separated using a magnet, and dried under vacuum at 60 °C. The exact amount of 4-aminoquinaldine grafted on silica-coated magnetic nanoparticles was determined via back titration by Mohr's method. The calculation revealed that  $0.93 \text{ mmol g}^{-1}$  of 4-aminoquinaldine is grafted on the surface of magnetic nanoparticles. Therefore, the use of

1 mmol of 4-aminoquinaldine is sufficient for the preparation of these modified nanoparticles but using the slight excess amount is necessary.

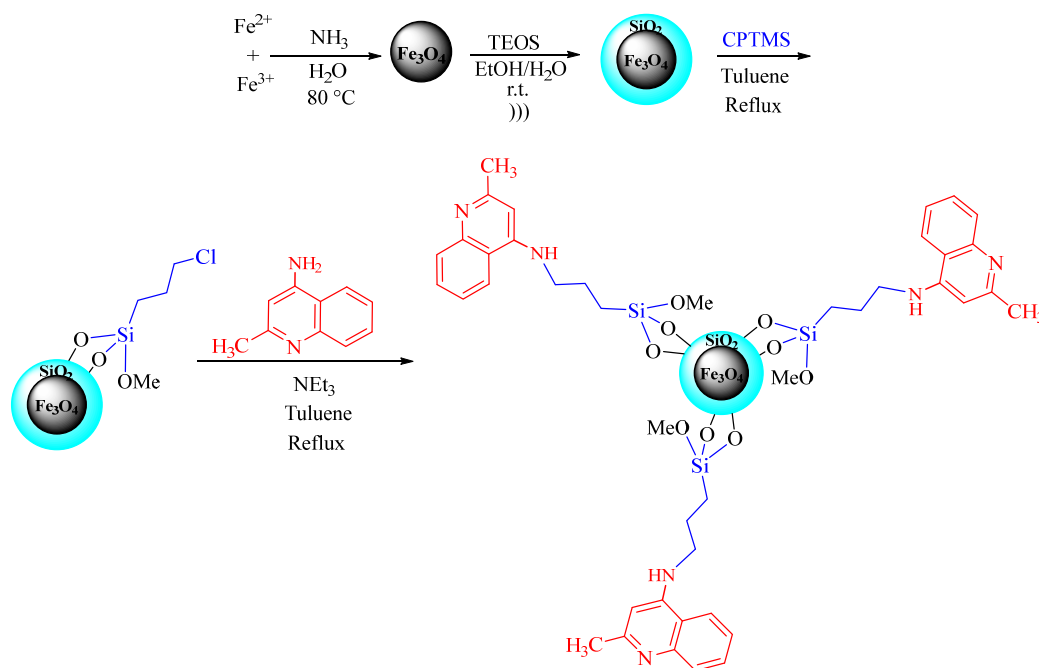
### 2.5. Synthesis of 2-amino-4H-chromenes in solvent-free conditions

A solution of aldehydes (1 mmol), malononitrile (0.066 g, 1 mmol),  $\alpha$ -naphthol/ $\beta$ -naphthol/phenol (1 mmol) and  $Fe_3O_4@SiO_2$ -AQ (0.05 g) was stirred at 100 °C temperature (Table 2). After completion of the reaction as monitored by TLC, the reaction mixture was dissolved in hot ethanol and was stirred for five minutes. The catalyst easily separated by means of an external magnet to be reused in subsequent reaction. The obtained products recrystallized in ethanol and characterized.

## 3. Results and Discussion

### 3.1. Preparation of nanomaterial ( $Fe_3O_4@SiO_2$ -AQ) as a novel hybrid nanocatalyst

The magnetic nanoparticle supported 4-aminoquinaldine catalyst ( $Fe_3O_4@SiO_2$ -AQ) was prepared via sequential reactions as shown in Scheme 2. Magnetite ( $Fe_3O_4$ ) nanoparticles were easily prepared via the chemical co-precipitation of  $Fe^{2+}$  and  $Fe^{3+}$  ions in basic solution [35]. These were subsequently coated with silica layer ( $Fe_3O_4@SiO_2$ ) through the well-known Stober method [36].



**Scheme 2.** Schematic steps for preparation of novel basic hybrid nanomaterial ( $Fe_3O_4@SiO_2$ -AQ).

The  $\text{Fe}_3\text{O}_4@\text{SiO}_2$  core-shell structures were treated with 3-chloropropyltrimethoxysilane (CPTMS), which can bind covalently to the free-OH groups at the particles surface and afforded the  $\text{Fe}_3\text{O}_4@\text{SiO}_2\text{-PrCl}$ . 4-aminoquinoline grafted on silica-coated magnetite nanoparticles ( $\text{Fe}_3\text{O}_4@\text{SiO}_2\text{-AQ}$ ) prepared with the reaction of the 3-chloropropyl-functionalized silica-coated magnetic nanoparticles ( $\text{Fe}_3\text{O}_4@\text{SiO}_2\text{-PrCl}$ ) and 4-aminoquinoline. The final hybrid nanomaterial was separated and washed with hot toluene and ethanol and then dried in a vacuum oven at 60 °C.

The FT-IR spectrum of  $\text{Fe}_3\text{O}_4$ ,  $\text{Fe}_3\text{O}_4@\text{SiO}_2$ ,  $\text{Fe}_3\text{O}_4@\text{SiO}_2\text{-PrCl}$ ,  $\text{Fe}_3\text{O}_4@\text{SiO}_2\text{-AQ}$  nanoparticles in the wavenumber range of 4000-400  $\text{cm}^{-1}$  is shown in Figure 1. The characteristic Fe-O absorption near 578  $\text{cm}^{-1}$  appeared in the FT-IR spectrum of magnetic  $\text{Fe}_3\text{O}_4$  nanoparticles (Fig. 1a) [37a]. The FT-IR spectrum of  $\text{Fe}_3\text{O}_4@\text{SiO}_2$  nanoparticles displays bands at about 1087 (asymmetric stretching), 955 (symmetric stretching), 781 (in plane bending) and 461  $\text{cm}^{-1}$  (rocking mode) of the Si-O-Si group and confirm the formation of  $\text{SiO}_2$  shell (Fig. 1b) [18, 23]. The broad peaks in the range 3200-3500  $\text{cm}^{-1}$  (Si-OH stretching vibration mode) and the weak peak at 1639  $\text{cm}^{-1}$  (twisting vibration mode of H-O-H adsorbed in the silica shell) are obvious in the spectrum. The weak aliphatic vibrations at 2933 and

2940  $\text{cm}^{-1}$  (Fig. 1c and 1d) related to C-H symmetric and asymmetric stretching and confirmed the presence of the attached alkyl groups. The peaks correspond to C=N and C=C in heterocyclic rings are appeared at 1400-1600  $\text{cm}^{-1}$  (Fig. 1d). N-H bending appeared at 1647  $\text{cm}^{-1}$  (Fig. 1d) [37b]. Therefore, the above results prove that the functional groups were successfully grafted onto the surface of the magnetic  $\text{Fe}_3\text{O}_4@\text{SiO}_2$  nanoparticles and resulted the final  $\text{Fe}_3\text{O}_4@\text{SiO}_2\text{-AQ}$  nanoparticles.

The size and morphology of the  $\text{Fe}_3\text{O}_4@\text{SiO}_2\text{-AQ}$  nanoparticles are detected by field-emission scanning electron microscope (FE-SEM) (Fig. 2). As you can see, the size of nanoparticles is 25-35 nm. Due to small size of the particles, the ratio of the surface to the volume of these particles is high, so more contact with the reactants take place and its catalytic role played well.

In order to investigate the nanoparticles and obtain information on morphology, size or shape of them was used for transmission electron microscopy. As shown in Fig. 3, the structure of the magnetic nanoparticles  $\text{Fe}_3\text{O}_4@\text{SiO}_2\text{-AQ}$  is almost spherical. In addition, the image shows a dark core ( $\text{Fe}_3\text{O}_4$ ) enclosed by a gray silica layer of thickness 5-10 nm. The average particles size is detected using a TEM image about 20-30 nm.

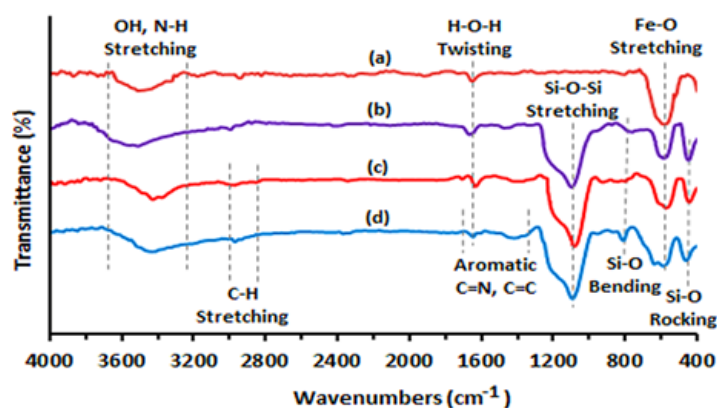


**Fig. 1.** The FT-IR spectrum of (a)  $\text{Fe}_3\text{O}_4$ , (b)  $\text{Fe}_3\text{O}_4@\text{SiO}_2$ , (c)  $\text{Fe}_3\text{O}_4@\text{SiO}_2\text{-PrCl}$ , and (d)  $\text{Fe}_3\text{O}_4@\text{SiO}_2\text{-AQ}$ .

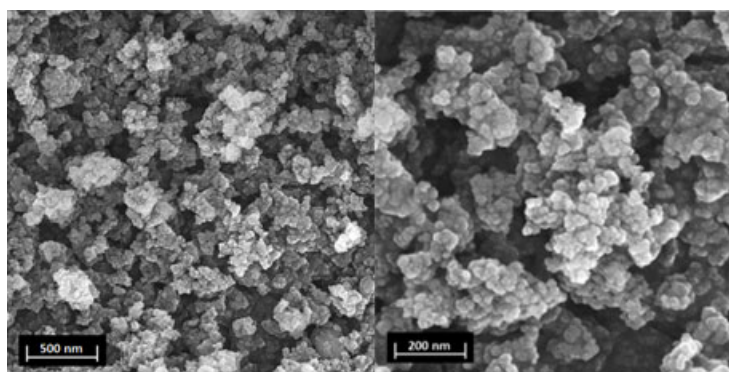


**Fig. 2.** FE-SEM images of  $\text{Fe}_3\text{O}_4@\text{SiO}_2\text{-AQ}$  nanoparticles.

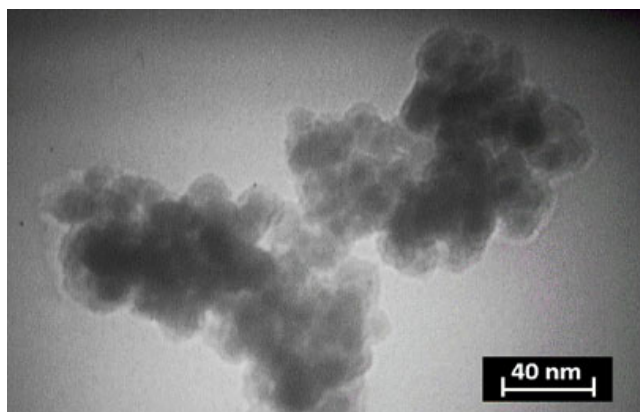


Fig. 3. TEM image of Fe<sub>3</sub>O<sub>4</sub>@SiO<sub>2</sub>-AQ nanoparticles.

The result of the X-ray diffraction (EDX) of the MNPs-AQ nanoparticles show the presence of C, N, Si and Fe signals. As expected, the peaks around 0.8 (Fe-L $\alpha$ ), 6.4 (Fe-K $\alpha$ ), and 7.0 (Fe-K $\beta$ ) keV are related to the binding energies of Fe. The higher peak intensity of Si element compared to Fe peak indicates that Fe<sub>3</sub>O<sub>4</sub> nanoparticles are trapped by SiO<sub>2</sub> and confirms the synthesized core-shell structure. According to these analyzes, it can be concluded that the Fe<sub>3</sub>O<sub>4</sub>@SiO<sub>2</sub>-AQ nanoparticles has been successfully synthesized (Fig. 4). The amount of 4-aminoquinaldine grafted onto the Fe<sub>3</sub>O<sub>4</sub>@SiO<sub>2</sub> was calculated through the following equation [37c, 37d], using the nitrogen content of Fe<sub>3</sub>O<sub>4</sub>@SiO<sub>2</sub>-AQ from EDS analysis (Eq. 1):

$$\text{mol g}^{-1} = \frac{\frac{[W_t \times 100]}{X} \times \left[ \frac{100}{100 - \left( \frac{W_t \times 100}{X} \right)} \right]}{Y} \quad (1)$$

Where  $W_t$  is the weight percent of the element measured,  $X$  is the theoretical weight percent of the element in the molecule and  $Y$  is the theoretical molecular weight of the molecule. 4-aminoquinaldine has nitrogen contents of 17.71 wt% with  $M_w$  of 158.20 g mol<sup>-1</sup>. Based on this equation, the amount of 4-aminoquinaldine detected from the nitrogen content is 0.0085 mol g<sup>-1</sup>.

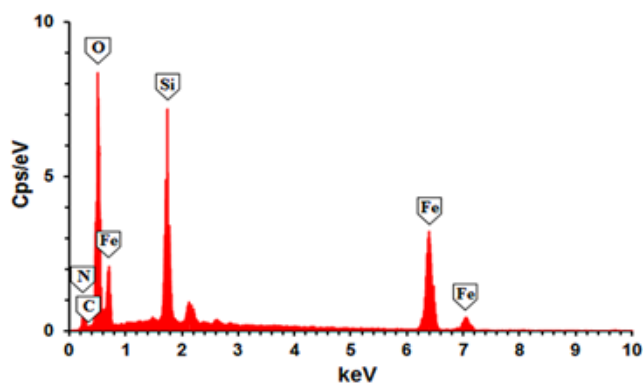


Fig. 4. The EDX spectrum of Fe<sub>3</sub>O<sub>4</sub>@SiO<sub>2</sub>-AQ nanocatalyst.

The presence and degree of crystallinity of magnetic Fe<sub>3</sub>O<sub>4</sub> and the Fe<sub>3</sub>O<sub>4</sub>@SiO<sub>2</sub>-AQ catalyst was considered from XRD measurements (Fig. 5). The same peaks were observed in the both of the magnetic Fe<sub>3</sub>O<sub>4</sub> and Fe<sub>3</sub>O<sub>4</sub>@SiO<sub>2</sub>-AQ XRD patterns, indicating retention of the crystalline spinel ferrite core structure during the silica-coating and functionalization processes. The XRD data of the synthesized magnetic nanoparticles show diffraction peaks at  $2\theta = 30.4^\circ, 35.8^\circ, 43.3^\circ, 53.9^\circ, 57.3^\circ, 63^\circ,$  and  $74.5^\circ$  which can be assigned to the (220), (311), (400), (422), (511), (440) and (533) planes of Fe<sub>3</sub>O<sub>4</sub>, respectively, indicating that the Fe<sub>3</sub>O<sub>4</sub> particles in the nanoparticles were pure Fe<sub>3</sub>O<sub>4</sub> with a cubic spinel structure; these matches well with the standard Fe<sub>3</sub>O<sub>4</sub> sample (JCPDS card no. 85-1436). The broad peak from  $2\theta = 20^\circ$  to  $27^\circ$  (Fig. 5b) is consistent with an amorphous silica phase in the shell of the silica-coated Fe<sub>3</sub>O<sub>4</sub> nanoparticles (Fe<sub>3</sub>O<sub>4</sub>@SiO<sub>2</sub>) [38]. The (311) XRD peak was used to estimate the average crystallite size of the magnetic nanoparticles by Scherrer's equation ( $D = 0.9\lambda/\beta \cos \theta$ ), where  $D$  is the average crystallite size,  $\lambda$  is the X-ray wavelength (0.154 nm),  $\beta$  denotes the full width in radians subtended by the half maximum intensity width of the (311) powder peak, and  $\theta$  corresponds to the Bragg angle of the (311) peak in degrees [39a]. From the width of the peak at  $2\theta = 35.7^\circ$  (311), the crystallite size of the magnetic nanoparticle is calculated to be 20.1 nm using Scherrer's equation, which is in near range of the size determined by FE-SEM analysis (Fig. 2).

The stability of the Fe<sub>3</sub>O<sub>4</sub>@SiO<sub>2</sub>-AQ catalyst was determined by thermogravimetric analysis (TGA) and derivative thermogravimetry (DTG) (Fig. 6). The magnetic catalyst shows two step weight loss steps over the temperature range of TG analysis (Fig. 6). The first stage, including a low amount of weight loss (2 %) at  $T < 250^\circ\text{C}$ , is due to the removal of physically adsorbed

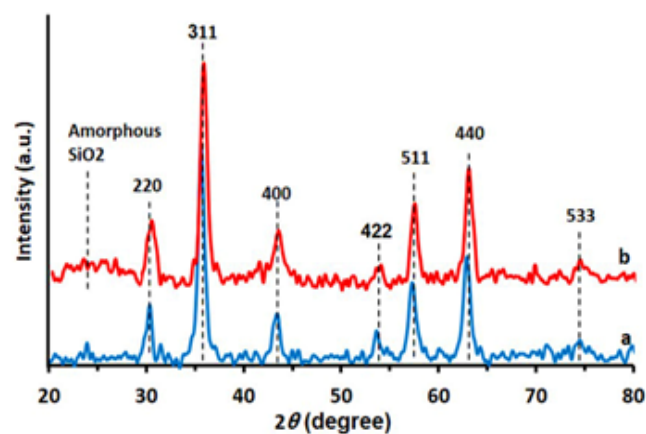


Fig. 5. The XRD patterns of (a) Fe<sub>3</sub>O<sub>4</sub> MNPs and (b) Fe<sub>3</sub>O<sub>4</sub>@SiO<sub>2</sub>-AQ.

solvent and surface hydroxyl groups, the second stage at about 250 °C to nearly 520 °C is attributed to the decomposition of the organic moiety in the nanocomposite. Therefore, the weight loss between 250-520 °C gives the organic grafting ratios of the magnetic catalyst. The grafted organic moiety on the magnetic  $\text{Fe}_3\text{O}_4@\text{SiO}_2$  nanoparticles was approximately 22 wt%. Therefore, it can be concluded that approximately the surface of the sample is covered by organic agents. In accordance with this mass loss, it was calculated that 0.8 mmol of 4-aminoquinoline was loaded on 1 g of  $\text{Fe}_3\text{O}_4@\text{SiO}_2$ -AQ catalyst and are accessible for catalytic reaction processes [39b]. Therefore, the  $\text{Fe}_3\text{O}_4@\text{SiO}_2$ -AQ is stable around or below 250 °C.

The magnetic properties of nanoparticles were measured by VSM (magnetic vibration measurement). Figure 7 illustrates the magnetic nanoparticle curve at the room temperature, which contains the magnetization (M) against magnetic field (H) (hysteresis loops) of  $\text{Fe}_3\text{O}_4$ ,  $\text{Fe}_3\text{O}_4@\text{SiO}_2$ -AQ. The hysteresis curve provides important information about magnetic properties such as the saturation magnetization ( $M_s$ ), remanent magnetization ( $M_r$ ) and coercivity ( $H_c$ ). It is obvious that by increase the magnetic field, the magnetization increases rapidly and it fixed in the 10000 Oe field and the sample is saturated completely. As shown in the Fig. 7, the  $M_s$  of  $\text{Fe}_3\text{O}_4@\text{SiO}_2$ -AQ is altered from  $64 \text{ emu g}^{-1}$  to  $42 \text{ emu g}^{-1}$  because the silica shell is formed around the  $\text{Fe}_3\text{O}_4$ . The hysteresis curve indicates the super paramagnetic properties for  $\text{Fe}_3\text{O}_4$ ,  $\text{Fe}_3\text{O}_4@\text{SiO}_2$ -AQ which the  $M_r$  and  $H_c$  are near the zero [40].

### 3.2. Catalytic studies of $\text{Fe}_3\text{O}_4@\text{SiO}_2$ -AQ

The catalytic activity of this novel hybrid nanocatalyst has been appraised for the synthesis of 4*H*-chromenes (Scheme 3). The reaction of 4-chlorobenzaldehyde, 2-

naphthol, malononitrile in the presence of a catalyst was selected as the model reaction and parameters affecting the reaction yields such as temperature, solvent, catalyst amount, and the solvent-free conditions were investigated (Table 1). As shown in Table 1, conventional heating at 120 °C under solvent-free condition is more efficient (Table 1, entry 11) over the organic solvents, because of its considerable efficiency and environmental compatibility.

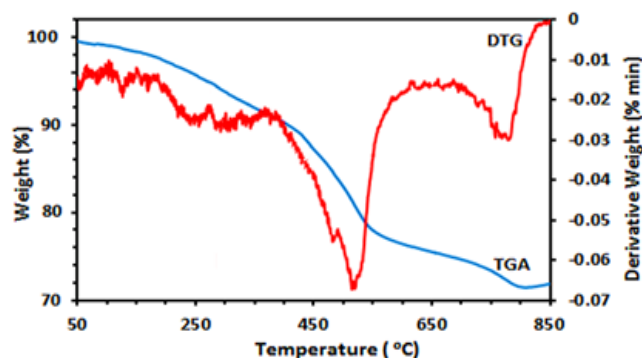


Fig. 6. The TGA-DTA curves of  $\text{Fe}_3\text{O}_4@\text{SiO}_2$ -AQ nanoparticles.

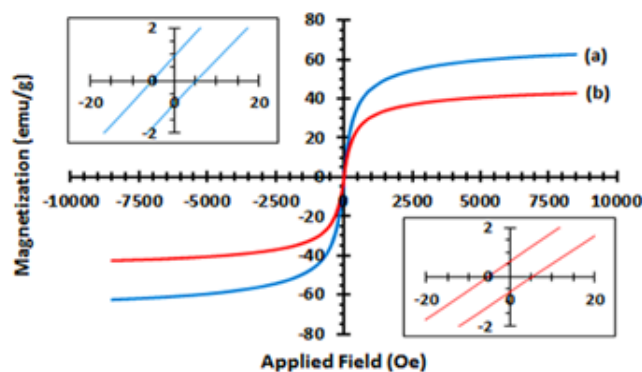
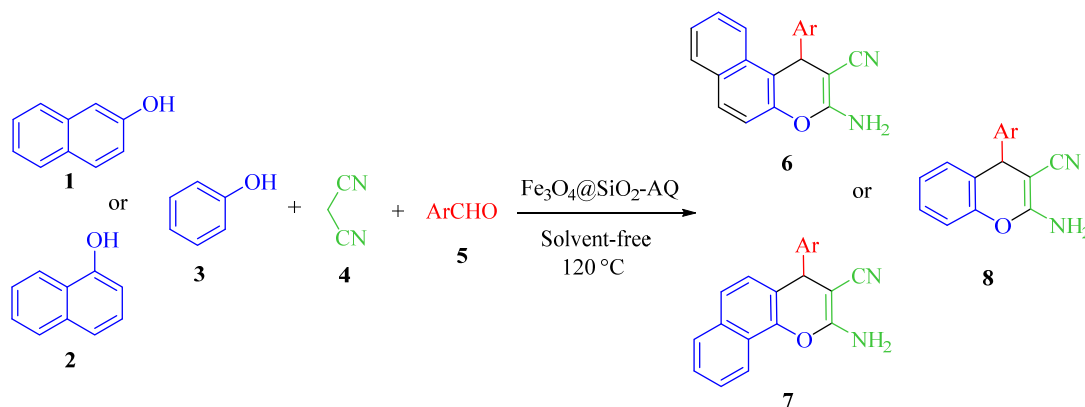
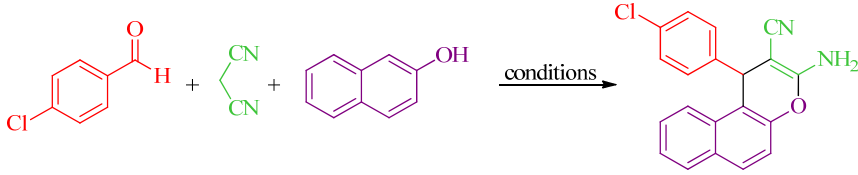


Fig. 7. The Magnetic hysteresis loops of (a)  $\text{Fe}_3\text{O}_4$  MNPs and (b)  $\text{Fe}_3\text{O}_4@\text{SiO}_2$ -AQ.



Scheme 3.  $\text{Fe}_3\text{O}_4@\text{SiO}_2$ -AQ as a hybrid nanocatalyst for efficient synthesis of 4*H*-chromene derivatives.

**Table 1.** Optimization of reaction conditions for preparation of 4*H*-chromene derivatives.


No.	Catalyst (mg)	Solvent	Temp. (°C)	Time (min)	Yield (%) <sup>a</sup>
1	Fe <sub>3</sub> O <sub>4</sub> @SiO <sub>2</sub> -AQ (30)	CH <sub>3</sub> CN	Reflux	120	47
2	Fe <sub>3</sub> O <sub>4</sub> @SiO <sub>2</sub> -AQ (30)	CH <sub>2</sub> Cl <sub>2</sub>	Reflux	150	36
3	Fe <sub>3</sub> O <sub>4</sub> @SiO <sub>2</sub> -AQ (30)	THF	Reflux	150	53
4	Fe <sub>3</sub> O <sub>4</sub> @SiO <sub>2</sub> -AQ (30)	Toluene	Reflux	180	23
5	Fe <sub>3</sub> O <sub>4</sub> @SiO <sub>2</sub> -AQ (30)	H <sub>2</sub> O	Reflux	60	57
6	Fe <sub>3</sub> O <sub>4</sub> @SiO <sub>2</sub> -AQ (30)	EtOH	Reflux	60	74
7	Fe <sub>3</sub> O <sub>4</sub> @SiO <sub>2</sub> -AQ (50)	EtOH:H <sub>2</sub> O	Reflux	60	81
8	Fe <sub>3</sub> O <sub>4</sub> @SiO <sub>2</sub> -AQ (50)	Solvent-free	50	60	48
9	Fe <sub>3</sub> O <sub>4</sub> @SiO <sub>2</sub> -AQ (50)	Solvent-free	80	60	59
10	Fe <sub>3</sub> O <sub>4</sub> @SiO <sub>2</sub> -AQ (50)	Solvent-free	100	45	81
11	Fe <sub>3</sub> O <sub>4</sub> @SiO <sub>2</sub> -AQ (50)	Solvent-free	120	30	93
12	Fe <sub>3</sub> O <sub>4</sub> @SiO <sub>2</sub> -AQ (30)	Solvent-free	120	30	84
13	-	Solvent-free	120	120	17
14	Fe <sub>3</sub> O <sub>4</sub> (30)	Solvent-free	120	120	37
15	Fe <sub>3</sub> O <sub>4</sub> @SiO <sub>2</sub> (30)	Solvent-free	120	120	41

<sup>a</sup>Isolated yields.

With the optimized conditions in hand, malononitrile and different substituted aldehydes were reacted with  $\beta$ -naphthol,  $\alpha$ -naphthol or phenol in the multicomponent one-pot reaction to obtain substituted 2-amino-4*H*-chromenes derivatives. The results were summarized in Tables 2. These reactions were very efficient and the desired products were obtained in good to excellent yields (81–96%) in relatively short reaction times, without formation of byproducts. Arylaldehydes with electron-donating or electron-withdrawing groups could lead to the favorite products with no reasonable difference in their reactivity. Aliphatic aldehydes were also used, but did not afford desired products in good yields.

### 3.3. Catalyst recovery

The recovery and reusability of the catalyst are very important for commercial and industrial applications as well as green process considerations. Thus, the recovery and reusability of Fe<sub>3</sub>O<sub>4</sub>@SiO<sub>2</sub>-AQ was investigated in the sequential reaction of 4-chlorobenzaldehyde (1 mmol), malononitrile,  $\beta$ -Naphthol and Fe<sub>3</sub>O<sub>4</sub>@SiO<sub>2</sub>-AQ (50 mg) as catalyst in solvent-free condition for 30 min.

After completion of the reaction, the resulting solidified mixture was diluted with hot EtOH (15 mL). Then, the catalyst was easily separated using an external magnet, washed with hot EtOH, dried under vacuum and reused in a subsequent reaction. Nearly quantitative recovery of catalyst (up to 97%) could be obtained from each run. As seen in Fig. 8, the recycled catalyst could be reused six times without any additional treatment and appreciable reduction in catalytic activity. The recovered catalyst after six runs had no obvious change in structure, as shown by comparison of the FT-IR spectra to that of fresh catalyst (Fig. 9). The consistent structure and activity of recovered Fe<sub>3</sub>O<sub>4</sub>@SiO<sub>2</sub>-AQ catalyst indicates that the reused Fe<sub>3</sub>O<sub>4</sub>@SiO<sub>2</sub>-AQ also shows excellent performance for the synthesis of 4*H*-chromenes.

To demonstrate the applicability of prepared catalyst, the condensation reaction of benzaldehyde, malononitrile and  $\beta$ -naphthol under optimized conditions for synthesis of 4*H*-chromene derivatives was compared with other catalysts reported in literature (Table 3).

**Table 2.** Multicomponent one-pot synthesis of 4*H*-chromene derivatives.

Product	Ar	Phenolic compound	Time (min)	Yield (%) <sup>a</sup>	m.p. (°C) <sup>b</sup>		TON <sup>c</sup>	TOF <sup>d</sup>	Ref
					Found	Reported			
<b>4a</b>	C <sub>6</sub> H <sub>5</sub>	β-Naphthol	30	96	292-294	297-299	192	384	[43]
<b>4b</b>	3-NO <sub>2</sub> -C <sub>6</sub> H <sub>4</sub>	β-Naphthol	40	93	191-193	189-190	186	279	[45]
<b>4c</b>	4-NO <sub>2</sub> -C <sub>6</sub> H <sub>4</sub>	β-Naphthol	30	95	188-189	187-189	190	380	[41]
<b>4d</b>	4-Cl-C <sub>6</sub> H <sub>4</sub>	β-Naphthol	30	93	202-204	204-206	186	372	[41]
<b>4e</b>	2-Cl-C <sub>6</sub> H <sub>4</sub>	β-Naphthol	45	87	204-205	207-208	174	232	[44]
<b>4f</b>	4-F-C <sub>6</sub> H <sub>4</sub>	β-Naphthol	40	91	229-230	233-234	182	273	[46]
<b>4g</b>	4-CH <sub>3</sub> -C <sub>6</sub> H <sub>4</sub>	β-Naphthol	40	87	259-260	255-256	174	261	[43]
<b>4h</b>	4-OH-C <sub>6</sub> H <sub>4</sub>	β-Naphthol	60	91	247-249	246-248	182	182	[43]
<b>4i</b>	3-OH-C <sub>6</sub> H <sub>4</sub>	β-Naphthol	60	90	278-279	280-282	180	180	[45]
<b>4j</b>	4-OMe-C <sub>6</sub> H <sub>4</sub>	β-Naphthol	50	89	187-189	190-192	178	214	[42]
<b>4k</b>	4-N(Me) <sub>2</sub> -C <sub>6</sub> H <sub>4</sub>	β-Naphthol	40	92	230-232	225-228	184	276	[43]
<b>4l</b>	2-Thienyl	β-Naphthol	60	81	240-241	-	162	162	-
<b>4m</b>	Terphthaldehyde	β-Naphthol	60	90	275-278	-	180	180	-
<b>5a</b>	C <sub>6</sub> H <sub>5</sub>	α-Naphthol	30	96	185-187	178-180	192	384	[41]
<b>5b</b>	4-Cl-C <sub>6</sub> H <sub>4</sub>	α-Naphthol	40	93	237-239	230-232	186	279	[41]
<b>5c</b>	2-Cl-C <sub>6</sub> H <sub>4</sub>	α-Naphthol	40	90	231-233	236-237	180	270	[42]
<b>5d</b>	4-Br-C <sub>6</sub> H <sub>4</sub>	α-Naphthol	40	91	240-242	239-241	182	273	[45]
<b>5e</b>	4-OH-C <sub>6</sub> H <sub>4</sub>	α-Naphthol	40	90	193-196	190-192	180	270	[41]
<b>5f</b>	4-NO <sub>2</sub> -C <sub>6</sub> H <sub>4</sub>	α-Naphthol	30	95	231-233	233-235	190	380	[46]
<b>5g</b>	3-NO <sub>2</sub> -C <sub>6</sub> H <sub>4</sub>	α-Naphthol	40	91	217-218	214-215	182	273	[46]
<b>5h</b>	4-CH <sub>3</sub> -C <sub>6</sub> H <sub>4</sub>	α-Naphthol	30	92	209-210	204-206	184	368	[41]
<b>5i</b>	4-OMe-C <sub>6</sub> H <sub>4</sub>	α-Naphthol	50	90	193-195	190-191	180	216	[46]
<b>6a</b>	C <sub>6</sub> H <sub>5</sub>	Phenol	45	92	207-209	210-211	184	245	[48]
<b>6b</b>	4-Cl-C <sub>6</sub> H <sub>4</sub>	Phenol	45	93	180-182	178-180	186	248	[49]
<b>6c</b>	4-CH <sub>3</sub> -C <sub>6</sub> H <sub>4</sub>	Phenol	45	90	161-163	165-167	180	240	[49]
<b>6d</b>	3-OH-C <sub>6</sub> H <sub>4</sub>	Phenol	45	88	221-223	218-220	176	234	[49]
<b>6e</b>	Isophthaldehyde	Phenol	45	83	203-205	-	166	221	-

<sup>a</sup>Isolated yields.<sup>b</sup>Melting points were not corrected.<sup>c</sup>Turn over number (TON) based on the number of mole of isolated product.<sup>d</sup>Turn over frequencies (TOF)= TON/time (h).

As can be seen, the catalytic system reported in this research has some benefits in terms of simple condition, reaction time and yield and is better or comparable procedure for synthesis of 4*H*-chromenes.

#### 4. Conclusions

In this work, the 4-aminoquinaldine-functionalized silica coated magnetite nanoparticles (Fe<sub>3</sub>O<sub>4</sub>@SiO<sub>2</sub>-AQ) successfully prepared and used as a heterogeneous hybrid nanocatalyst for one-pot synthesis of substituted 2-amino-4*H*-chromenes. 4*H*-chromene derivatives were

prepared in high yields without using harmful solvents (under solvent-free condition). The prepared catalyst can be easily separated and recovered from the reaction system by a magnet, and can be reused for several times without significant loss of its activity. In addition, the method presents various advantages including high yields, operational simplicity, clean reaction conditions and minimum pollution of the environment, which makes it an effective and attractive procedure for the synthesis of these chromene derivatives and comparable with those reported in literature.

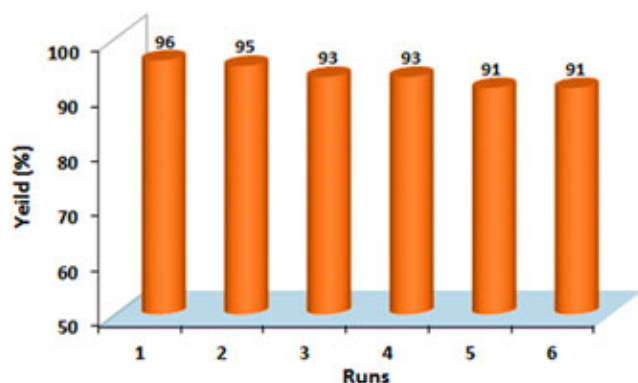


**Fig. 8.** The recyclability of Fe<sub>3</sub>O<sub>4</sub>@SiO<sub>2</sub>-AQ in the synthesis of 4*H*-chromenes.

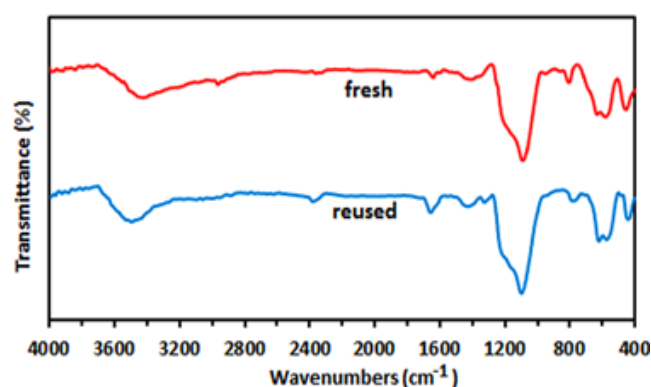


**Fig. 9.** The FT-IR spectra of fresh catalyst (Fe<sub>3</sub>O<sub>4</sub>@SiO<sub>2</sub>-AQ) and that reused six times.

**Table 3.** Comparison of Fe<sub>3</sub>O<sub>4</sub>@SiO<sub>2</sub>-AQ with other catalysts described in the literature for synthesis of 2-amino-4*H*-chromene via three-component reaction.<sup>a</sup>

Entry	Catalyst	Condition	Time (min)	Yield <sup>b</sup> (%)	Ref.
1	nanoeolite CP	H <sub>2</sub> O, Reflux	20	95	[41]
2	Ionic liquid	MW	7	87	[42]
3	MNPs-SPAsp	Solvent-free (120 °C)	30	93	[43]
4	CTABr	US, H <sub>2</sub> O	150	78	[44]
5	Nano MgO	H <sub>2</sub> O-PEG	60	84	[45]
6	<b>Fe<sub>3</sub>O<sub>4</sub>@SiO<sub>2</sub>-AQ</b>	<b>Solvent-free (100 °C)</b>	<b>30</b>	<b>96</b>	<b>Present work</b>

<sup>a</sup>Reaction conditions: β-Naphthol (1 mmol), malononitrile (1 mmol), benzaldehyde (1 mmol), and catalyst.

## Acknowledgements

The authors gratefully acknowledge the financial support of this work by the research council of Arak University.

## References

- [1] J. Zhu, Q. Wang, M.-X. Wang, *Multicomponent Reactions in Organic Synthesis*. 1st Edition, Wiley-VCH, Weinheim, Germany, 2015.
- [2] J. Zhu, H. Bienayme, *Multicomponent Reactions*. 1st Edition, Wiley-VCH, Weinheim, Germany, 2005.
- [3] J. Montgomery, *Acc. Chem. Res.* 33 (2000) 467-473.
- [4] H. Bienayme, K. Bouzid, *Angew. Chem., Int. Ed.* 37 (1998) 2234-2237.
- [5] (a) R. V. Orru, M. de Greef, *Synthesis* 10 (2003) 1471-1499. (b) L. Chen, X.-J. Huang, Y.-Q. Li, W.-J. Zheng, *Monatsh. Chem.* 140 (2004) 45-47.
- [6] L. F. Tietze, A. Modi, *Med. Res. Rev.* 20 (2000) 304-322. (b) S. J. Mohr, M. A. Chirigos, F. S. Fuhrman, J. W. Pryor, *Cancer Res.* 35 (1975) 3750-3754.
- [7] A. Kakanejadifard, F. Azarbani, N. Khosravani, B. Notash, *J. Mol. Liq.* 221 (2016) 211-215.
- [8] N. Seshu Babu, N. Pasha, K. T. Venkateswara Rao, P. S. Sai Prasad, N. Lingaiah, *Tetrahedron Lett.* 49 (2008) 2730-2733.
- [9] S. Zavar, *Arab. J. Chem.* 10 (2017) S67.
- [10] B. Wu, X. Gao, Z. Yan, M.-W. Chen, Y.-G. Zhou, *Org. Lett.* 17 (2015) 6134-6137.
- [11] G.-D. Yin, T.-T. Lai, Z.-S. Yan, H. Chen, J. Zheng, Q. Tao, *Tetrahedron* 69 (2013) 2430-2435.
- [12] G. Yin, H. Shi, L. Xu, X. Wei, Q. Tao, *Synthesis* 45 (2013) 334-340.
- [13] A. F. Mahmoud, A. El-Latif, F. Fathy, A. M. Ahmed, *Chin. J. Chem.* 28 (2010) 91-96.
- [14] A. Shaabani, R. Ghadari, S. Ghasemi, M. Pedarpour, A. H. Rezayan, A. Sarvary, S. W. Ng, *J. Comb. Chem.* 11 (2009) 956-959.
- [15] M. Fallah, Sh. Sohrabnezhad, M. Abedini, *Appl. Organomet. Chem.* 33 (2019) e4801.
- [16] W. MA, A-Gh. Ebadi, M. Shahbazi sabil, R. Javahershenas, G. Jimenez, *RSC Adv.* 9 (2019) 12801-12812.
- [17] A. Poursattar Marjani, B. Ebrahimi Saatluo, F. Nouri, *Iran. J. Chem. Chem. Eng.* 37 (2018) 149-157.
- [18] P. Gholamzadeh, G. M. Ziarani, N. Lashgari, A. Badiiei, P. Asadiatouei, *J. Mol. Catal. A: Chem.* 391 (2014) 208-222.

- [19] H. R. Shaterian, M. Mohammadnia, *J. Mol. Liq.* 177 (2013) 353-360.
- [20] S. Thadkapally, A. C. Kunjachan, R. S. Menon, *Beilstein J. Org. Chem.* 12 (2016) 16-21.
- [21] Ch. V. Subbareddy, Sh. Sumathi, *New J. Chem.* 41 (2017) 9388-9396.
- [22] K. Kantharaju, S. Y. Khatavi, *ChemistrySelect* 3 (2018) 5016-5024.
- [23] W. Injumba, P. Ritprajak, N. Insin, *J. Magn. Magn. Mater.* 427 (2017) 60-66.
- [24] S. H. Araghi, M. H. Entezari, *Appl. Surf. Sci.* 333 (2015) 68-77.
- [25] M. A. Bodaghifard, M. Hamidinasab, N. Ahadi, *Curr. Org. Chem.* 22 (2018) 234-267.
- [26] M. B. Gawande, P. S. Branco, R. S. Varma, *Chem. Soc. Rev.* 42 (2013) 3371-3393.
- [27] J.A. Gladysz, *Chem. Rev.* 102 (2002) 3215-3216.
- [28] V. Polshettiwar, R. Luque, A. Fihri, H. Zhu, M. Bouhrara, J. M. Basset, *Chem. Rev.* 111 (2011) 3036-3075.
- [29] S. Shylesh, V. Schünemann, W. R. Thiel, *Angew. Chem. Int. Edit.* 49 (2010) 3428-3459.
- [30] Y. Leng, K. Sato, Y. Shi, J. G. Li, T. Ishigaki, T. Yoshida, H. Kamiya, *J. Phys. Chem. C* 113 (2009) 16681-16685.
- [31] A. L. Morel, S. I. Nikitenko, K. Gionnet, A. Wattiaux, J. Lai-Kee-Him, C. Labrugere, B. Chevalier, G. Deleris, C. Petibois, A. Brisson, M. Simonoff, *ACS Nano* 2 (2008) 847-856.
- [32] M. A. Bodaghifard, A. Mobinikhaledi, S. Asadbegi, *Appl. Organometal. Chem.* 31 (2017) e3557.
- [33] M. A. Bodaghifard, S. Asadbegi, Z. Bahrami, *J. Iran. Chem. Soc.* 14 (2017) 365-376.
- [34] M. A. Bodaghifard, A. Mobinikhaledi, M. Hamidinasab, *Synth. React. Inorg. Met.-Org. Nano-Metal. Chem.* 44 (2014) 567-571.
- [35] K. Can, M. Ozmen, M. Ersoz, *Colloids Surf. B Biointerfaces* 71 (2009) 154-159.
- [36] W. Stöber, A. Fink, E. Bohn, *J. Colloid Interface Sci.* 26 (1968) 62-69.
- [37] (a) R. Sen, P. Jain, R. Patidar, S. Srivastava, R. Rana, N. Gupta, *Mater. Today* 2 (2015) 3750-3757. (b) M. K. Marchewka, *Mat. Sci. Eng. B* 95 (2002) 214-221. (c) M. Sarvestani, R. Azadi, *Appl. Organometal. Chem.* 31 (2017) e3667. (d) R. Nielsen, P. Kingshott, T. Uyar, J. Hacaloglu, K. L. Larsen, *Surf. Interface Anal.* 43 (2011) 884-892.
- [38] G. Feng, D. Hu, L. Yang, Y. Cui, X.-A. Cui, H. Li, *Sep. Purif. Technol.* 74 (2010) 253-260.
- [39] (a) J. Giri, S.G. Thakurta, J. Bellare, A. K. Nigam, D. Bahadur, *J. Magn. Magn. Mater.* 293 (2005) 62-68. (b) G. Alva, X. Huang, L. Liu, G. Fang, *Appl. Energy* 203 (2017) 677-685.
- [40] K. Petcharoen, A. Sirivat, *Mat. Sci. Eng. B* 177 (2012) 421-427.
- [41] S. M. Baghbanian, N. Rezaei, H. Tashakkorian, *Green Chem.* 15 (2013) 3446-3458.
- [42] A. Kumbhar, S. Jadhav, R. Shejwal, G. Rashinkar, R. Salunkhe, *RSC Adv.* 6 (2016) 19612-19619.
- [43] A. Mobinikhaledi, H. Moghanian, M. Ghanbari, *Appl. Organometal. Chem.* 32 (2018) e4108.
- [44] T. S. Jin, J.C. Xiao, S. J. Wang, T. S. Li, *Ultrason. Sonochem.* 11 (2004) 393-397.
- [45] T. S. Jin, J. S. Zhang, L. B. Liu, A. Q. Wang, T. S. Li, *Synth. Commun.* 36 (2006) 2009-2015.
- [46] D. Kumar, V. B. Reddy, G. B. Mishra, R. K. Rana, M. N. Nadagouda, R. S. Varma, *Tetrahedron* 63 (2007) 3093-3097.
- [47] H. Mehrabi, N. Kamali, *J. Iran. Chem. Soc.* 9 (2012) 599-605.
- [48] H. Yan, J. Zhang, C. You, Z. Song, B. Yu, Y. Shen, *Mater. Chem. Phys.* 113 (2009) 46-52.
- [49] R. Magar, P. Thorat, V. Jadhav, S. Tekale, S. Dake, B. Patil, R. Pawar, *J. Mol. Catal. A: Chem.* 118 (2013) 374-375.